Investigating Membrane Breakdown of Neuronal Cells Exposed to Nonuniform Electric Fields by Finite-Element Modeling and Experiments

Tjitske Heida*, Joost B. M. Wagenaar, Wim L. C. Rutten, and Enrico Marani

***Abstract*—High electric field strengths may induce high cell membrane potentials. At a certain breakdown level the membrane potential becomes constant due to the transition from an insulating state into a high conductivity and high permeability state. Pores are thought to be created through which molecules may be transported into and out of the cell interior. Membrane rupture may follow due to the expansion of pores or the creation of many small pores across a certain part of the membrane surface. In nonuniform electric fields, it is difficult to predict the electroporated membrane area. Therefore, in this study the induced membrane potential and the membrane area where this potential exceeds the breakdown level is investigated by finite-element modeling. Results from experiments in which the collapse of neuronal cells was detected were combined with the computed field strengths in order to investigate membrane breakdown and membrane rupture.**

It was found that in nonuniform fields membrane rupture is position dependent, especially at higher breakdown levels. This indicates that the size of the membrane site that is affected by electroporation determines rupture.

***Index Terms*—Electropermeabilization, electroporation, finite-element modeling, membrane breakdown, nonuniform electric fields.**

I. Introduction

In order to trap cortical rat neurons by dielectrophoretic forces a nonuniform electric field is needed [1], [2]. However, high electric field strengths may lead to membrane breakdown possibly resulting in cell death. It was already shown that cells trapped at 3 V_{pp}/14 MHz, resulting in a maximum field strength of 109 kV/m, remained viable and did not show morphological changes [3]. Furthermore, with increasing frequency a higher breakdown potential was found for frequencies ranging from 10 kHz to 1 MHz. The aim of this paper is to investigate membrane breakdown and cell rupture due to high electric field strengths by experiments and finite-element modeling. First, a short overview of membrane breakdown and electroporation is given.

Membrane breakdown is the phenomenon by which the membrane of biological cells can be brought into a high-conductivity state when large membrane potentials are induced by an external electric field [4]. Other terms to express the same phenomenon are *electroporation* or *electropermeabilization*. It can be used for many clinical purposes like the introduction of DNA, enzymes, antibodies, and other biochemical reagents for intracellular assays [4]. However, the occurrence of membrane breakdown is an inevitable side-effect when exposing biological cells to high electric field strengths for dielectrophoretic manipulation of cells (e.g., cell trapping and cell separation).

A. Membrane Potential

The proteins embedded in the lipid bilayer mainly determine the electrical properties of cell membranes [5]. Functional proteins such as ion "pumps" are involved in maintaining ion concentration differences, which in turn determine the membrane potential. The maintenance of a set membrane potential is of importance in controlling the amplitude of nerve impulses (action potentials) and muscle contractions.

Often a cell can be represented by a single-shell model, meaning that it consists of a homogeneous sphere, the cytoplasm, surrounded by a thin shell, the membrane. Living cells have an interior (cytoplasm) whith a high conductivity (due to an accumulation of ions such as K^+) and an average dielectric constant a little lower than that of surrounding aqueous medium. Under dc field application a membrane potential is induced. When assuming that this field is homogeneous, that the resting membrane potential is superimposed on the field induced membrane potential and it is not changed by the external field, and that surface admittance and space charge effects do not play a role, the membrane potential can be calculated according to [5], [6]

$$V_m = f_s E r \cos\alpha \pm V_{\text{rest}} \tag{1}$$

with E the static electric field, V_{rest} the resting membrane potential, r the cell radius, α the angle between the field line and a normal from the center of the sphere to a point of interest on the membrane (the maximal transmembrane potential is induced at the membrane patch facing an electrode, $\alpha = 0°$ or 180°), and f_s is a function reflecting the electrical and dimensional properties of the cell and the surrounding medium; f_s can be calculated

Manuscript received January 2, 2001; revised May 9, 2002. *Asterisk indicates corresponding author.*

*T. Heida is with the Institute of BioMedical Technology, Department of Biomedical Engineering, Faculty of Electrical Engineering, University of Twente, P.O. Box 217, 7500 AE Enschede, The Netherlands (e-mail: t.heida@el.utwente.nl).

J. B. M. Wagenaar and W. L. C. Rutten are with the Institute of BioMedical Technology, Department of Biomedical Engineering, Faculty of Electrical Engineering, University of Twente, 7500 AE Enschede, The Netherlands.

E. Marani is with the Neuroregulation Group, Department of Neurosurgery, Faculty of Medicine, University of Leiden, 2300 RC Leiden, The Netherlands.

Publisher Item Identifier 10.1109/TBME.2002.803503.

according (2), shown at the bottom of the page, where σ_{med}, σ_{int}, and σ_{mem} are the electric conductivities of the medium, of the cytoplasm, and of the membrane, respectively, and d is the membrane thickness.

Equation (1) can be simplified under the following assumptions:

1) the membrane conductivity σ_{mem} can be neglected;
2) the membrane thickness d is much smaller than the cell radius r;
3) when the induced membrane potential is sufficiently high the resting membrane potential can be neglected.

Then holds [5], [7]

$$V_m = 1.5Er\cos\alpha. \tag{3}$$

When an alternating (sinusoidal) electric field with amplitude E is applied, the generated membrane potential is given by the following equation [5], [7], [8]

$$V_m = \frac{1.5Er\cos\alpha}{\sqrt{1+(2\pi f\tau)^2}} \tag{4}$$

with f the frequency of the field. The time constant τ of the membrane can be written as

$$\tau = rC_{\mathrm{mem}}\left(\frac{1}{\sigma_{\mathrm{int}}}+\frac{1}{2\sigma_{\mathrm{med}}}\right) \tag{5}$$

with R_{mem} and C_{mem} the specific resistance and capacitance per unit area, respectively.

Equations (3) and (4) indicate that the induced membrane potential increases with increasing cell radius. It is, therefore, assumed that the cell organelles are unaffected by the breakdown of the cell membrane. The single-shell model is, therefore, valid for the investigation of membrane breakdown.

Under nonuniform field conditions the membrane potential at which breakdown occurs becomes unpredictable. The theory presented above is applicable only for small external, uniform electric fields. When large transmembrane potentials are induced the theory fails [9]. The charging transient is interrupted and the membrane potential becomes nearly constant at about 0.2–1 V [5], [10]–[13], which is most apparent at the poles of the cell and the cosinusoidal profile of the induced potential around the cell is, therefore, lost. At this point *membrane breakdown* or *electropermeabilization* occurs resulting in an increased membrane conductivity. The specific conductivity of the cell membrane can rise form about 10^{-3} S/m^2 to more than $10 * 10^3$ S/m^2 [13], [14].

B. Pulse Length and Temperature Dependence

The high permeability state caused by dielectric breakdown is dependent on the amplitude and duration of the electric field as well as on temperature and medium conductivity [5], [11]–[13], [15]. For example, at a pulse length of 10 μs the breakdown potential of is of the order of 0.5 V; it rises to approximately 1.2 V for a pulse length of 800 ns. These values apply to the situation in which the temperature was about 25°C. A pulse length of several hundred ns at 4°C resulted in a breakdown potential of 2 V, while at 40°C it is only 0.5 V [5], [11].

C. Pore Model

The high permeability state was hypothesized to be caused by microscopic membrane perforations, or pores, that allow transport of ions and molecules across the membrane [13], [16].

Lipid bilayers have a central, nonpolar, layer which is about 2–3 nm thick. Such a thin sheet of low permittivity ($\varepsilon \sim 2$) excludes ions and charged molecules. The electrostatic energy needed to move charge from a high dielectric medium (such as water, $\varepsilon_{\mathrm{water}} = 80$) into a low dielectric medium, termed the Born energy, is large due to the large difference in permittivities of both materials [14]. The energy needed to insert a small ion into a membrane is significantly reduced if the ion is placed into a (mobile) aqueous cavity or if it can pass through an aqueous channel, i.e., aqueous pathways [16]. The greater reduction is achieved by the pore and is, therefore, assumed to form the basis of electroporation/electropermeabilization. The conductance of the bilayer itself is so small that the conductance is entirely due to that of the pores, which is greatly determined by the number of pores.

A heterogeneous distribution of pore sizes is expected due to thermal fluctuations and variations in electric field energy within the membrane [16]. The minimum pore size, R_{min}, is about 1 nm; thus, the small ions that comprise physiologic saline can be transported through the pores. Additionally, a critical radius, R_c, exists meaning that a pore of that size will spontaneously grow and this would rupture the membrane.

Larger membrane potentials, such as those near the poles according to (3) and (4), produce more pores to shunt the extra stimulus current across the membrane [9]. Increasing the electric field strength results in a larger fraction of the cell membrane being electroporated. However, only a small fraction of the membrane surface is generally affected. For example, the maximum fractional area of the membrane occupied by the pores was found to be about 10^{-4} to 10^{-3} [9].

The mechanism by which molecular transport occurs during electroporation is not fully understood yet. Electrophoresis, diffusion, and endocytosis are possible mechanisms [4].

With the aqueous pore theory the transient response of the cell membrane to an electrical pulse can be described. It consists of the following chronological phases [15], [17], [18].

- The increase in membrane conductance appears immediately or a few milliseconds after the pulse.
- Expansion/evolution of the pores appears during the first few milliseconds at a rate of 3.1–7.3 pA/ms.

$$f_s = \frac{3\sigma_{\mathrm{med}}\left[3dr^2\sigma_{\mathrm{int}} + \left(3d^2r - d^3\right)\left(\sigma_{\mathrm{mem}} - \sigma_{\mathrm{int}}\right)\right]}{2r^3\left(\sigma_{\mathrm{mem}} + 2\sigma_{\mathrm{med}}\right)\left(\sigma_{\mathrm{mem}} + 0.5\sigma_{\mathrm{int}}\right) - 2\left(r-d\right)^3\left(\sigma_{\mathrm{med}} - \sigma_{\mathrm{mem}}\right)\left(\sigma_{\mathrm{int}} - \sigma_{\mathrm{mem}}\right)} \tag{2}$$

- The high-conductance state of the membrane lasts up to about 100 ms.
- The recovery process consists of two subphases:
  fast recovery process (in the millisecond range): the conductance returns to the approximate prepulse level; pores shrink and partially reseal;
  slow recovery process (several seconds to minutes): the low-conductance state turns into a state with closed pores.

D. Electromechanical Model

In spite of the ability of the aqueous pore theory to explain the electropermeability state and its transience, this theory does not include electromechanical loading. Assuming that the membrane can be regarded as a capacitor filled with a homogeneous elastic dielectric material, it can be postulated that the thickness of the membrane capacitor depends on the electrical compressive and mechanical forces (e.g., internal hydrostatic pressure) [5]. For example, the Maxwell–Wagner interfacial depolarizations may result in deformation forces [19]. These effects may lead to changes in the membrane structure without the formation of distinct pores.

The electromechanical model is able to explain some of the observations that are difficult to interpret by the aqueous pore theory [5], [19].

- The dependence of the dipole generation on medium conductivity accounts for the observed dependence of electropermeabilization on medium conductivity;
- By assuming that the membrane material is not perfectly elastic and shows inertia, the pulse-length dependence of the breakdown potential can be explained. If the elastic compressive modulus transverse to the membrane plane is a function of the compression time, it increases with increasing rate of compression, comparable to other viscoelastic materials.

E. Recovery of the Membrane

The recovery process of the membrane was found to be temperature-dependent. For example, at 4 °C complete recovery may require about 30 min; at 20 °C–30 °C it may require significantly less [5].

The recovery of the membrane to its original low conductivity and low permeability state does not necessarily mean that the original membrane structure is completely restored [5]. Cell death may occur due to rupture of the membrane, or chemical imbalances resulting from influx and efflux during the high permeability state of the membrane [4].

F. Methods of Observation

The high permeability state of the membrane can most effectively be measured by staining the cell membrane with appropriate fluorescent-labeled dyes [5], [17], [20]. Visualization of pores by any present form of microscopy is unlikely, because of their small size and short lifetime [4], [5], [16]. To test "normal" functioning of the cell after field exposure, parameters like cell growth, division rates, viability and cell motility should be used as these integrate influences over long observation times.

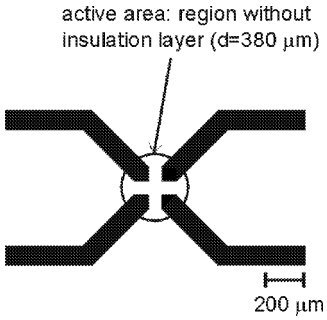

Fig. 1. Triangular electrode tips were used for the experiments. The diagonal inter-electrode distance was 100 μm.

II. METHODS

A. Planar Quadrupole Microelectrode Structure

The electrode plate consists of gold electrodes on a glass substrate of 5 by 5 cm and a thickness of 1 mm. The electrode tips were triangular as shown in Fig. 1. In [3], a detailed description of the fabrication procedure is given.

B. Electric Field Generation

The electric field was created using a sinusoidal signal from a HP 3245 A universal source. Amplitude and frequency were set via a computer according to a Labview script (LabVIEW 6.0, National Instruments LabVIEW™, 2000) in the range from 2 to 18 V_{pp}, and 100 kHz to 1 MHz, respectively.

C. Cells and Medium

Cells obtained exclusively from the telencephalic cortex of newborn rats (P2) were used for the experiments in this study. A detailed description of the dissociation procedure is given in [3]. The neurons were suspended in R12 medium [21], [22], which has a conductivity of 1.6 S/m, and the suspension used for the experiments consisted of about $1.5 * 10^6$ viable cells/ml.

D. Experimental Procedure

A drop of cell suspension was applied on top of an electrode structure. For 30 min the plate was set at rest, i.e., cells were allowed to precipitate randomly and adhere to the substrate. In order to investigate membrane breakdown, high field strengths are needed. Application of an electric field directs the cells to regions of minimal field strength by negative dielectrophoresis. Due to the adhesive forces the cells initially positioned close to the electrodes were, thus, not directly pushed away from the electrode when the field was applied.

After 30 min, the electrode plate was clamped into a small box in which small pins provide the connection from the gold electrodes to the coaxial cable leading to the signal generator. This box was directly placed on a Nikon Inverted microscope (Diaphot-TMD). Before an electric field was applied an image was taken from the cells by a digital camera (Sony CCD Camera, Model DXC-151P). The field was created by a sinusoidal signal from the generator via a Labview-script. The frequency was constant while the value of the signal was increased in steps of 0.5 V_{pp}, from 2 to 18 V_{pp}. Each value was applied during 14 s, i.e., 10 s and the time needed to take an image, which was about

4 s. Frequencies in the range from 100 kHz to 1 MHz were used. Previous experiments showed that preservation of cell viability is largely frequency and amplitude dependent in this range.

Membrane rupture or cell collapse could be detected with phase contrast microscopy. The moment a neuronal cell collapses it turns dark, comparable to the uptake of a staining substance like Trypan Blue. Experiments were performed in which some of the electrode structures were covered with a normal cell suspension, while other were covered with a drop of cell suspension to which a small drop of Trypan Blue (about 4 μl) was applied. These experiments confirmed that the use of phase contrast microscopy made the process of cell collapse visible with equal precision as compared to detecting the uptake of Trypan Blue.

E. Data Analysis Procedure

The first and last images were used to identify ten cells that collapsed, while they stayed on the same position during the experiment. From the first image, the diameter of these cells was determined which was assumed to remain constant until collapse. For each of the identified cells the point at which collapse occurred was detected by passing through all images. Each image is related to a certain amplitude of the input signal and, thus, to a certain electric field strength near the cell. From the first image, a point on the cell was indicated as being the membrane site at which the induced membrane potential was largest. The field intensity at this point was determined by finite-element modeling, as described in the next paragraph, from which the membrane potential can be calculated according to (4), assuming $\cos\alpha = 1$ (the profile of the membrane potential around the cell does not comply to a cosinus function in the case of nonuniform fields). It has to be noted that the membrane probably had already adopted a high permeability state at this point and, therefore, the calculated potential will tend to be higher than the factual breakdown level.

For the graphical presentation of the results the percentage of cells that had collapsed was determined as a function of the membrane potential. The potential was taken from 0 to 2 V with intervals of 0.1 V. For each interval, we checked how many cells had collapsed. This was done for each frequency.

III. Finite-Element Model

Finite-element modeling can be used to determine the electric field inside a three-dimensional medium. A cell can be introduced into the model by modeling it as a sphere with homogeneous properties. The surface area of this sphere, which is shared by the surrounding medium and the sphere, is meshed. This meshed area can be copied and can be used for the definition of a new sphere. This sphere is the cytoplasm. The first sphere is deleted while keeping the area mesh on the medium intact. There are now two layers of nodes with exactly the same positions, however they are not connected. One layer belongs to the medium and one layer belongs to the cell interior (Fig. 2). Between two nodes located at the same position circuit elements can be introduced. These represent the membrane. The membrane consists of a resistance in parallel with a capacitance. Each node covers a small part of the spherical surface and this area

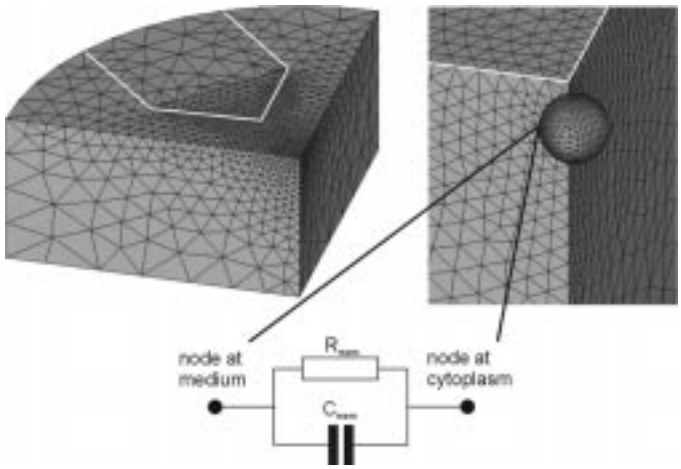

Fig. 2. "Element plot" of the cell and the surrounding medium (bottom view). A submodel consisting of a quarter of the complete electrode structure was used for accurate computation of the electric field around the cell and the corresponding induced membrane potential. White lines indicate the contour of the electrode tip. On the right, a part of the electrode tip with the cell is presented. The lower figure shows the parallel combination of a resistance and capacitance representing the membrane, which created the connection between two nodes located at the same position, i.e., the node at the medium and the node at the cytoplasm.

determines the local resistivity and capacity of the membrane ($R_{\mathrm{mem}} = 0.1\ \Omega\mathrm{m}^2$, $C_{\mathrm{mem}} = 9\ \mathrm{mF/m}^2$). The complete model includes all four electrodes. Therefore, after simulation of the complete model a second simulation was performed using a submodel, which consists of a quarter of the model. Element sizes could be scaled down with this submodel so that a high accuracy was attained in the computation of the electric field around the cell and the induced membrane potential. Fig. 2 shows the elements of the submodel. The internode-distance at the cell surface was 0.5 μm. At the sides of the electrodes the internode-distance was about 1.5 μm. Element size increased with increasing distance from the electrode edges and the cell as shown in Fig. 2.

Areas represented the electrodes since their actual height was only 0.4 μm. Applying a potential of -2.5 and $+2.5$ V per two electrodes opposing each other the potential distribution and the electric field can be computed. The potential difference over the parallel combination of membrane resistance and capacitance represents the membrane potential. Using this potential as input signal in the same model the membrane potential distribution can be determined.

Since the area of membrane breakdown is strongly dependent on local electric field intensities a cell located at the tip or along the side of the electrode was expected to show different results in breakdown experiments. Fig. 3 shows the locations of the two cells; two models were used each including one cell.

A. Modeling Results

Fig. 4 shows the computed electric field distribution created by the quadrupole electrode structure in the xy-plane at $z = 0$ μm for 5 V_{pp}, while no cell was included. With a cell located just above the electrode tip the electric field is disturbed according to Fig. 5. At low frequencies the membrane completely blocks the electric field, while at frequencies above 1 MHz the membrane potential drops and the field penetrates the cell interior.

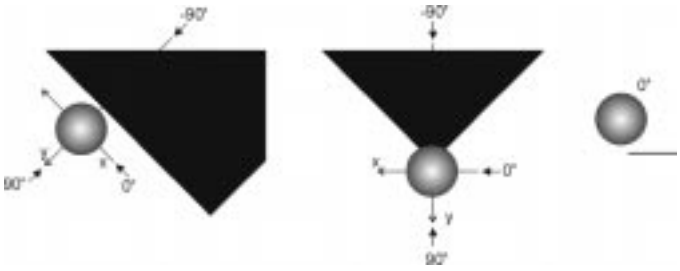

Fig. 3. (a) Cell at the side of the electrode tip with the center of the cell at $z = 7$ μm. (b) Cell at the electrode tip with the center of the cell at $z = 8$ μm. (c) Side view of the cell above the electrode. For both situations the cell radius was 6 μm. Three viewing directions are indicated as $-90°$, $0°$, and $90°$. These were used for the presentation of the results in Fig. 5.

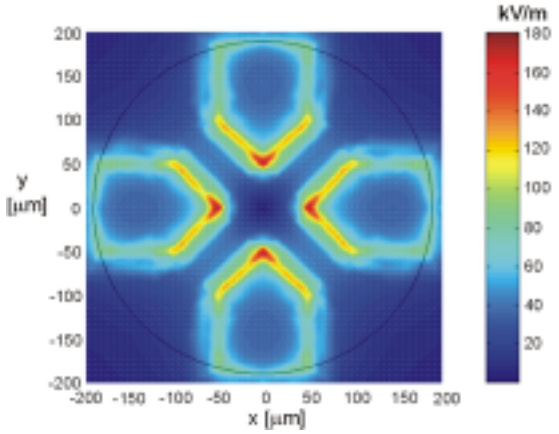

Fig. 4. Electric field distribution created by a quadrupole electrode structure with triangular electrode tips in the horizontal plane at $z = 0$ μm.

As expected, at the higher field strength near the tip of the electrode a larger induced membrane potential was found (Fig. 6). In addition, the variation in membrane potential is largest for the cell at the tip due to the large field gradient. Only at a small part of the membrane a large membrane potential is induced. Fig. 7 shows the area of the membrane for which the membrane potential exceeds a certain threshold (the total membrane surface for a cell with a radius of 6 μm is 452 $*10^{-12}$ m^2). The amplitude of the threshold ranges from 0.2 to 1 V.

While for a cell located along the side of the electrode the maximum membrane potential was 0.75 V the total area affected by the field was equal in size as the area for a cell located at the tip for low threshold values (0.2–0.4 V).

IV. Experimental Results

Fig. 8 shows the experimental results for the experiment performed at 800 kHz. In general, cells located near an electrode collapse at lower field intensities in comparison to cells located further away. The cells had an average diameter of 10 μm (SD = 2).

In order to solve (4) to determine the membrane potential, the electric field strength generated by the electrode structure needs to be known. According to finite-element modeling, the maximum field strength was 181.09 kV/m for 5 V_{pp} (see Fig. 3). In practice, the calculated maximum field strengths were not realized due to nonideal material properties. Circuit simulation showed that even at high frequencies the maximum field strength induced in the medium was about 90% of the ideal value (not shown here). Table I gives the maximum field intensities per frequency as a percentage of the theoretical maximum field strength. Once the maximum electric field strengths are known, the maximum induced membrane potentials $V_{m,\max}$ can be calculated according to (4).

A. Membrane Potential

From the images, the membrane potentials were determined at the point that the cells collapsed. Each experiment contained ten cells of which membrane rupture occurred according to their location and cell radius (assuming the cells to be spherical). Fig. 9 shows the percentage of cells that has collapsed as a function of the membrane potential.

Most of the cells collapsed at a membrane potential of 0.4 V at 100 kHz. For higher frequencies the percentage of dead cells is smeared out over a range from 0.5 to about 1.1 for 250 and 800 kHz, and from 0.6 to 1.7 V for 1 MHz.

Cells were positioned randomly inside the active region. However, this random positioning of the ten cells under study has to be comparable for the four experiments. Fig. 10, therefore, shows the average distance of the membrane sites of the cells nearest to an electrode edge and the electrode edge as a function of frequency. No significant differences were found and, thus, the experiments are based on corresponding conditions.

V. Discussion

From literature, it may be expected that membrane breakdown leading to membrane rupture is dependent on a combination of the frequency of the field, temperature, the porated surface area of the membrane, and mechanical stress. Most of these parameters are dependent on the position of the cell inside the nonuniform electric field.

From the graph of Fig. 9, it is clear that a frequency dependency is present. This frequency dependency could be a direct result of the membrane area affected by electroporation. If a certain area needs to be electroporated before membrane rupture is induced much higher field strengths are needed at higher frequencies (Fig. 7).

The results for 100 kHz show that membrane rupture occurs at a membrane potential of about 0.4 V for all cells. Therefore, at 100-kHz membrane breakdown was nearly independent of the position and radius of the cell and, thus, of the area involved in electroporation. Fig. 7(a) versus Fig. 7(b) confirms that the position of the cell does not affect the area of membrane breakdown at the lower frequencies (10 and 100 kHz) for a breakdown level up to about 0.5 V; the 10- and 100-kHz curves are almost identical. When breakdown occurs at higher frequencies cell position starts to affect the membrane area involved in breakdown, especially with increasing membrane potentials (>0.5 V). A position dependent breakdown level may be the cause of the decrease in the steepness of the slopes of Fig. 9 with increasing frequency. It has to be noted that the two situations shown in

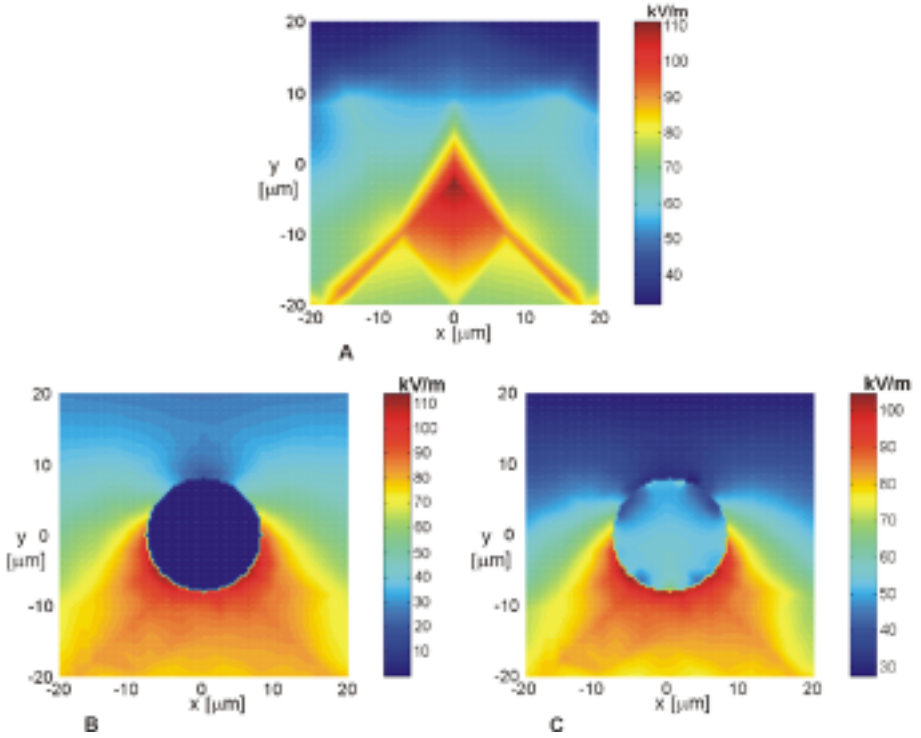

Fig. 5. Electric field in the xy-plane at $z = 8\ \mu$m (the center of the cell). The center of the cell was taken to be at the center of the coordinate system; the area shown ranges from $x = y = -20\ \mu$m to $x = y = 20\ \mu$m. (a) No cell was included. (b) Cell included and frequency was set at 10 kHz. (c) Cell included and frequency was set at 12 MHz.

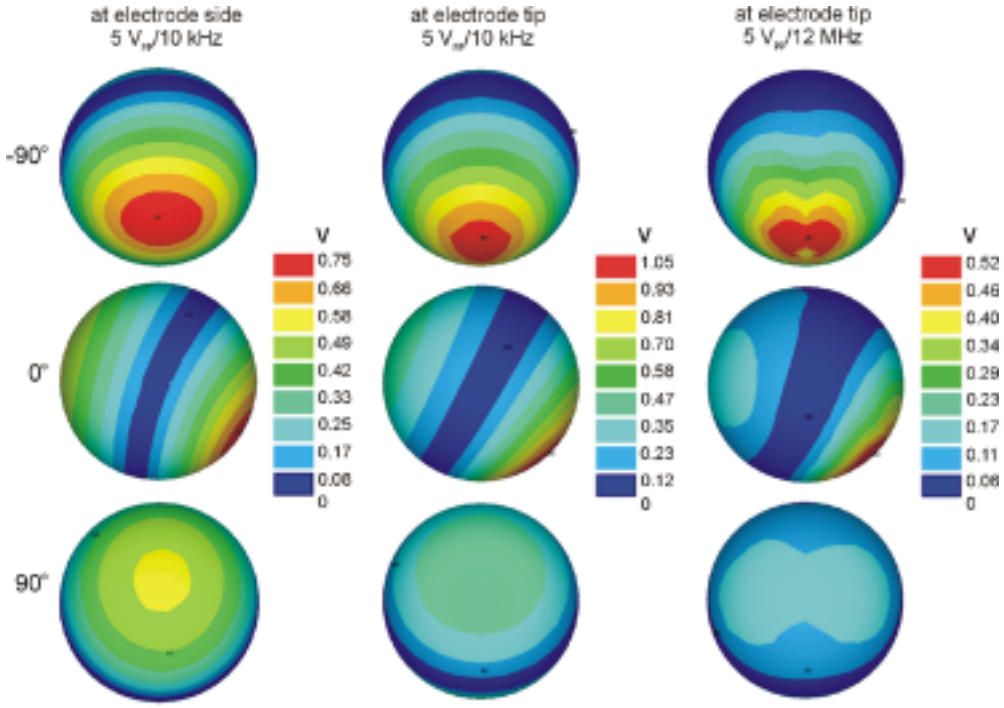

Fig. 6. Membrane potentials determined for (a) a cell positioned along the electrode side (5 V_{pp}/10 kHz), and (b) a cell positioned at the electrode tip at 5 V_{pp}/10 kHz, and (c) 5 V_{pp}/12 MHz.

Figs. 6 and 7 do not cover the complete scala of possible positions. They represent the "worst case" situations. It is however assumed that the relationship between electroporated membrane area and membrane potential will for most cells comply to the average of the curves of Fig. 7. Fig. 10 shows the average distance of the cells to the electrodes.

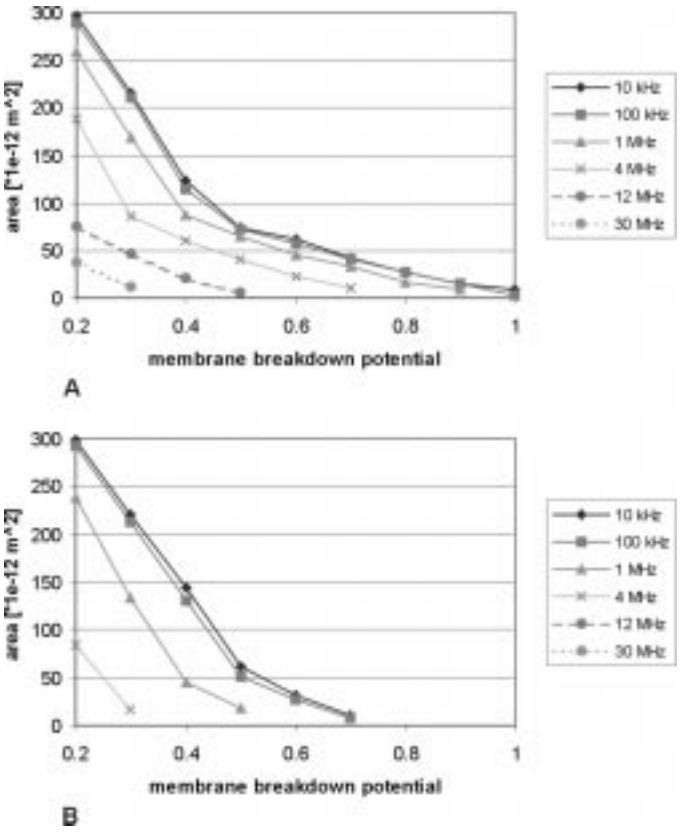

Fig. 7. Membrane area for which the membrane potential exceeds a certain value for a cell located at (a) the tip or (b) along the side of an electrode. The membrane potential ranges from 0.2 to 1 V.

TABLE I
PERCENTAGE OF THE FIELD STRENGTH IN RELATION TO THE THEORETICAL FIELD STRENGTH

frequency [kHz]	$\frac{E_{estimate}}{E_{theoretical}} * 100\%$
100	44%
250	70%
800	87%
1000	88%

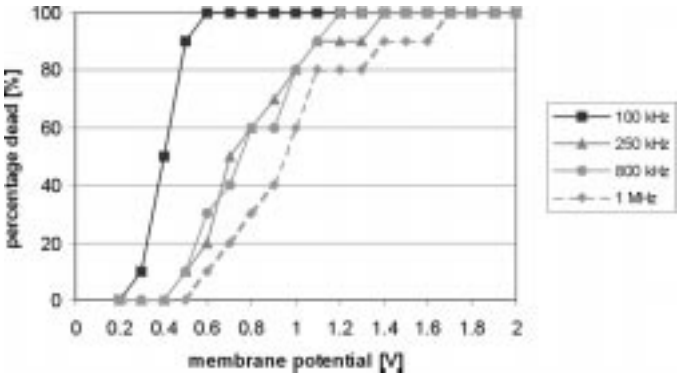

Fig. 9. Percentage of collapsed cells as a function of the induced membrane potential. Each graph consists of ten cells with varying diameter and located at different positions inside the field.

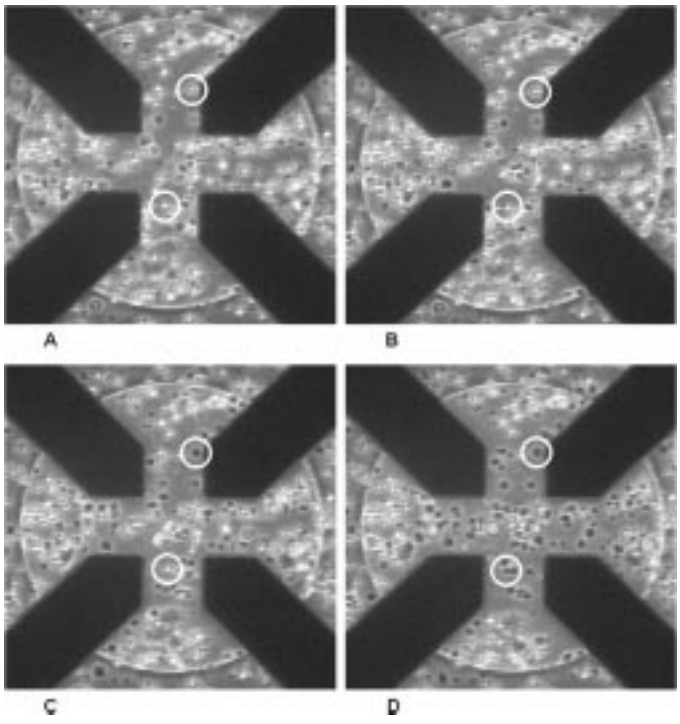

Fig. 8. Experimental results: situations at the start of the experiment [(a) (image0)], (b) 7 V_{pp}, (c) 12 V_{pp}, and (d) 17 V_{pp}. The frequency was set at 800 kHz. A white circle indicates two cells. At 12 V_{pp} the cell near the electrode (upper circle) has already collapsed; at 17 V_{pp} the other cell had also turned dark.

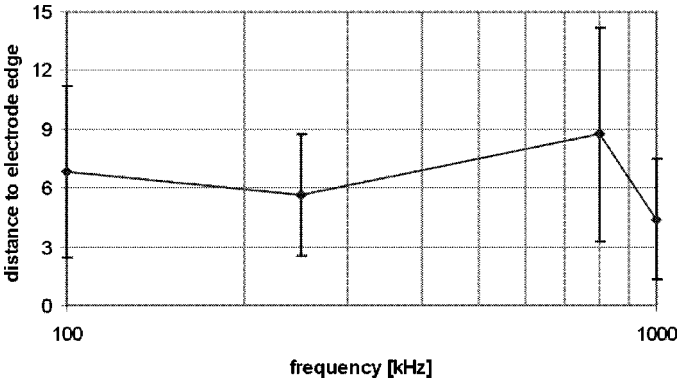

Fig. 10. Average distances between the membrane site of the cells nearest to an electrode edge and the electrode edge as a function of frequency.

It has to be kept in mind that both (4) used for the calculation of V_m, and the finite-element model are based on the assumption that the membrane capacitance is constant. The specific membrane capacitance is determined by the dielectric constant and thickness of the membrane. Protein content and lipid constituents largely determine these parameters. However, almost independent of the density of proteins in the membrane the specific capacitance of neuronal membranes was found to be 9 mF/m^2 [23]. The relaxation frequency for proteins and lipids is in the range 100 kHz–10 MHz [1]. Frequency dependency could, therefore, also be the result of additional dispersions in the membrane. However, protein dispersions are masked by the

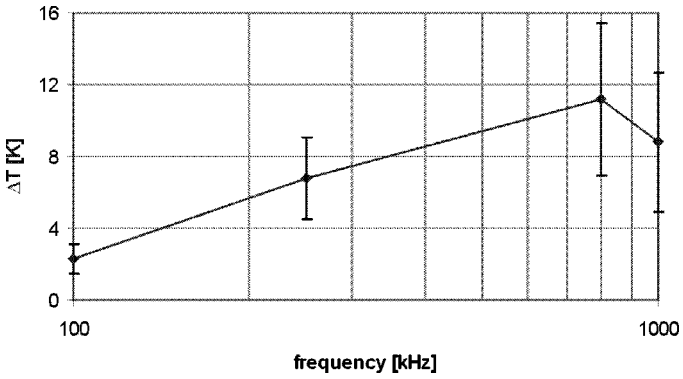

Fig. 11. Estimated average temperature rises for each frequency.

stronger β or Maxwell–Wagner dispersion [24]. Assuming a constant membrane permittivity and conductivity and, thus, the models used, are justified.

Mechanical stress on the cells arises from the electrical compressive forces on the membrane or from the pressure within ion channels to expand them [5]. These forces are hardly observable and are, therefore, omitted for discussion. Another mechanical force is created by the fluid flow arising from local heating of the medium. From previous experiments, it was found that a temperature rise of 1.5 °C occurred at an input signal of 5 V_{pp} at frequencies above 1 MHz. At lower frequencies smaller temperature variations were measured which can be ascribed to the reduced field strength as a result of the high electrode-medium impedance. A direct relation exists between temperature rise and input signal [25]

$$\frac{\Delta T_1}{\Delta T_2} = \frac{V_1^2}{V_2^2}. \tag{6}$$

For all four experiments an average input signal was determined at which breakdown occurred, incorporating the effect of the electrode-medium interface (Table I), from which the average temperature rise was estimated. The result is shown in Fig. 11.

From Fig. 11, it may be expected that at the higher frequencies the mechanical force due the fluid flow exerted on a cell may result in a lower breakdown level; the larger the temperature rise the larger the mechanical stress exerted on a cell by the created fluid flow. In addition, with increasing temperature the membrane breakdown level decreases [5], [11]. This might explain the overlapping breakdown levels for 250 and 800 kHz in Fig. 9. With increasing frequency an increase in breakdown level is expected. However, due to the temperature rise the breakdown level decreases, which might be the case for the experiment performed at 800 kHz. For the 1 MHz-experiment the frequency dependence dominates since the breakdown level was highest in this case.

In conclusion, modeling of the cell and the electric field in three dimensions may result in the ability to predict whether cells will survive exposure to the field or not and if this is dependent on the position of the cells in the nonuniform field and field frequency. The experimental results for nonuniform electric fields fit previous findings from literature for uniform fields [5], [9], [11]–[13]. In comparison with uniform fields, field frequency also greatly determines the breakdown level of the cell membranes in nonuniform fields. In addition, with increasing temperature the breakdown level is found to decrease.

While the cells have been modeled as being spherical the advantage of using of a finite-element method is that the cell may attain any shape. Freshly dissociated cortical neurons are almost spherical, however, when they adhere to a substrate their shape changes and membrane properties at the adhesion sites may even be changed. The consequence of such changes has not been investigated yet. However, the relationship between the cells as modeled in this study considering the membrane breakdown potential need not differ much when incorporating a modified cell shape.

Another advantage of using finite-element modeling is the creation of inhomogeneities inside the cell. However, since the interior of the cell is shielded by the membrane at frequencies below about 1 MHz, a nonhomogeneous cell interior may not significantly alter the results. In contrast, the addition of a surface conductance and/or space charges around the cell may greatly influence the membrane potential. This was already investigated analytically [26], and it can simply be modeled by adding a second shell to the model described above. Since the effects were negligible for high medium conductivities $(>1$ S/m$)$ [26] the single-shell model was considered to give a good representation of the neuron for the situation described in this study.

REFERENCES

[1] H. A. Pohl, *Dielectrophoresis*. Cambridge: Cambridge University Press, 1978.
[2] T. Heida, W. L. C. Rutten, and E. Marani, "Dielectrophoretic trapping of dissociated fetal cortical rat neurons," *IEEE Trans. Biomed. Eng.*, vol. 48, pp. 921–930, 2001a.
[3] ——, "Viability of dielectrophoretically trapped neural cortical cells in culture," *J. Neurosci. Meth.*, vol. 110, pp. 37–44, 2001b.
[4] J. C. Weaver, "Electroporation: A general phenomenon for manipulating cells and tissue," *J. Cell. Biochem.*, vol. 51, pp. 426–435, 1993.
[5] U. Zimmermann and G. A. Neil, *Electromanipulation of Cells*. Boca Raton, Florida: CRC Press, 1996.
[6] T. Kotnik, F. Bobanović, and D. Miklavčič, "Sensitivity of transmembrane voltage induced by applied electric fields—A theoretical analysis," *Bioelectrochem. Bioenerg.*, vol. 43, pp. 285–291, 1997.
[7] P. Marszalek, D.-S. Liu, and T. Y. Tsong, "Schwan equation and transmembrane potential induced by alternating electric field," *Biophys. J.*, vol. 58, pp. 1053–1058, 1990.
[8] H. P. Schwan, "Electrical properties of tissue and cell suspensions," in *Advances in Biological and Medical Physics*, J. H. Lawrence and E. Tobias, Eds. New York: Academic Press, 1957, vol. 5.
[9] K. A. DeBruin and W. Krassowska, "Modeling electroporation in a single cell. I. Effects of field strength and rest potential," *Biophys. J.*, vol. 77, pp. 1213–1224, 1999.
[10] J. Teissié and M.-P. Rols, "An experimental evaluation of the critical potential difference inducing cell membrane electropermeabilization," *Biophys. J.*, vol. 65, pp. 409–413, 1993.
[11] R. Benz and U. Zimmermann, "Pulse length dependence of the electrical breakdown in lipid bilayer membranes," *Biochim. Biophys. Acta*, vol. 597, pp. 637–642, 1980a.
[12] ——, "The resealing process of lipid bilayers after reversible electrical breakdown," *Biochim. Biophys. Acta*, vol. 640, pp. 169–178, 1980b.
[13] ——, "Relaxation studies on cell membranes and lipid bilayers in the high electric field range," *J. Electroanal. Chem.*, vol. 116, pp. 723–739, 1980c.
[14] H. B. L. Coster, "Self-assembly, stability and the electrical characteristics of cell membranes," *Aust. J. Phys.*, vol. 52, pp. 117–140, 1999.
[15] F. Ryttsén, C. Farre, C. Brennan, S. G. Weber, K. Nolkrantz, K. Jardemark, D. T. Chiu, and O. Orwar, "Characterization of single-cell electroporation by using patch-clamp and fluorescence microscopy," *Biophys. J.*, vol. 79, pp. 1993–2001, 2000.

[16] J. C. Weaver, "Electroporation theory," in *Methods in Molecular Biology*. Totowa, NJ: Humana Press Inc, 2000, vol. 47, Electroporation Protocols for Microorganizms.
[17] T. Y. Tsong, "Electroporation of cell membranes," *Biophys. J.*, vol. 60, pp. 297–306, 1991.
[18] D. C. Chang and T. S. Reese, "Changes in membrane structure induced by electroporation as revealed by rapid-freezing electron microscopy," *Biophys. J.*, vol. 58, pp. 1–12, 1990.
[19] V. L. Sukhorukov, H. Mussauer, and U. Zimmermann, "The effect of electrical deformation force on the electropermeabilization of erythrocyte membranes in low- and high-conductivity media," *J. Membrane Biol.*, vol. 163, pp. 235–245, 1998.
[20] S. Y. Ho and G. S. Mittal, "Electroporation of cell membranes: A review," *Crit. Rev. Biotech.*, vol. 16, pp. 349–362, 1996.
[21] H. J. Romijn, F. van Huizen, and P. S. Wolters, "Toward an improved serum-free, chemically defined medium for long-term culturing of cerebral cortex tissue," *Neurosci. and Biobehav. Rev.*, vol. 8, pp. 301–334, 1984.
[22] E. Marani, M. Corino, R. J. van den Berg, W. J. Rietveld, M. Deenen, and W. Windhorst, "Ionic conductances in cultured pre-infundibular cells from the hypothalamic arcuate region," *Neuroendocrinology*, vol. 48, pp. 445–452, 1988.
[23] L. J. Gentet, G. J. Stuart, and J. D. Clemens, "Direct measurement of specific membrane capacitance in neurons," *Biophys. J.*, vol. 79, pp. 314–320, 2000.
[24] J. Gimsa and D. Wachner, "A unified resistor-capacitor model for impedance, dielectrophoresis, electrorotation, and induced transmembrane potential," *Biophys. J.*, vol. 75, pp. 1107–1116, 1998.
[25] H. Glasser, T. Schnelle, T. Müller, and G. Fuhr, "Electric field calibration in micro-electrode chambers by temperature measurements," *Thermochimica Acta*, vol. 333, pp. 183–190, 1999.
[26] C. Grosse and H. P. Schwan, "Cellular membrane potentials induced by alternating fields," *Biophys. J.*, vol. 63, pp. 1632–1642.

Tjitske Heida received the M.Sc. and Ph.D. degrees in electrical engineering from the University of Twente, Enschede, The Netherlands, in 1997 and 2002, respectively. Her Ph.D. thesis concerns trapping neurons by dielectrophoretic forces.

She is currently working in the department of Measurement & Instrumentation at the same university. Her research interests were the investigation of dielectrophoresis of neurons and the effect of the nonuniform electric fields on the neurons, simulation of high-frequency electric fields in three dimensions by a finite-element method, and microelectrode design and fabrication.

Joost B. M. Wagenaar is a third-year student at the department of Electrical Engineering at the University of Twente, Enschede, The Netherlands.

His research concerning membrane breakdown of neuronal cells was based on an individual research assignment at the biomedical group of the university.

Wim L. C. Rutten was trained as an experimental physicist and received the Ph.D. degree in from the University of Leiden, Leiden, The Netherlands. Thereafter, he studied the auditory system at the ENT department of Leiden University Hospital.

Since 1985, he is an Assistant and Associate Professor of Biomedical Control Systems with BMTI/Faculty of Electrical Engineering, University of Twente, Enschede, The Netherlands. His present research interests are neural engineering and cellular engineering (neuro-electronic interfaces, cultured probes), signal processing, and bioelectricity.

Enrico Marani was trained as a Neuroanatomist and received the Ph.D. degree from the Leiden University, Leiden, The Netherlands, in 1982.

Thereafter, he became Head of the Neuroregulation group at the Department of Neurosurgery, Leiden University Medical Center. Since 1997, he has been a Part-time Professor of Neurophysiology at the BMTI/Faculty of Electrical Engineering of the University of Twente, Enschede, The Netherlands. His present research interests are neuroregulation and neurotechnology, especially in the field of nerve regeneration.